SPO2FRAG: Software for seismic fragility assessment based on static pushover

Georgios Baltzopoulos[1] • **Roberto Baraschino[2]** • **Iunio Iervolino[2]** • **Dimitrios Vamvatsikos[3]**

Abstract SPO2FRAG (Static PushOver to FRAGility) is introduced, a MATLAB®-coded software tool for estimating structure-specific seismic fragility curves of buildings, using the results of static pushover analysis. The SPO2FRAG tool (available online at http://wpage.unina.it/iuniervo) eschews the need for computationally demanding dynamic analyses by simulating the results of incremental dynamic analysis via the SPO2IDA algorithm and an equivalent single-degree-of-freedom approximation of the structure. Subsequently, fragility functions may be calculated for multiple limit states, using the intensity-measure-based analytical approach. The damage thresholds may also be random variables and uncertainty in estimation of the fragility parameters may be explicitly accounted for. The research background underlying the various modules comprising SPO2FRAG is presented together with an operational description of how the various functions are integrated within the software's graphical user interface. Two illustrative SPO2FRAG applications are also offered, using a steel and a reinforced concrete moment resisting frame. Finally, the software output is compared with the results of incremental dynamic analysis as validation of SPO2FRAG's effectiveness.

Keywords performance-based earthquake engineering, static non-linear methods, vulnerability.

1. INTRODUCTION

Performance-based earthquake engineering (PBEE) is a structural engineering paradigm that fully embraces the intrinsic uncertainty associated with strong ground motion and employs probabilistic tools to evaluate structural performance in seismic areas (e.g., Cornell and Krawinkler, 2000). Perhaps the most notable example is the problem of estimating the rate of earthquakes leading the structure to fail in meeting a performance objective (a situation often referred to as *exceedance of a limit state*). This calculation can be performed by an implementation of the total probability theorem:

$$\lambda_f = \int_{IM} P\left[f \,|\, IM = im \right] \cdot \left| d\lambda_{im} \right| \tag{1}$$

The terms appearing in the equation are the sought rate of failure, λ_f, the rate of exceeding a certain value of a ground motion intensity measure (IM), λ_{im}, and the conditional probability of failure given a certain level of seismic intensity, $P\left[f \,|\, IM = im \right]$; i.e., the fragility of the structure. The term λ_{im} is a measure of the seismic hazard at a specific site and can be evaluated by means of probabilistic seismic hazard analysis (note that the absolute value of the differential, $\left| d\lambda_{im} \right|$, appears in the equation).

The methods used to derive such fragility functions can be classified as empirical, analytical or hybrid; the interested reader is referred to Calvi et al. (2006) for a comprehensive overview. In recent

---

[1] Istituto per le Tecnologie della Costruzione, URT Università degli Studi di Napoli Federico II, Consiglio Nazionale delle Ricerche, Via Claudio 21, 80125 Naples, Italy.

[2] Dipartimento di Strutture per l'Ingegneria e l'Architettura, Università degli Studi di Napoli Federico II, Via Claudio 21, 80125 Naples, Italy.

[3] Department of Civil Engineering, National Technical University of Athens, 9 Heroon Politechneiou, 127 80 Athens, Greece.

years there has been considerable emphasis on the analytical approach, which is based on numerical models, especially for structure-specific fragility functions. State-of-the-art analytical methods rely on advanced numerical models of the structure subjected to nonlinear dynamic analyses. A classic example of such analysis is incremental dynamic analysis (IDA, Vamvatsikos and Cornell, 2002). IDA accounts for the variability of structural response (i.e., the so-called *record-to-record variability*) by using a sample of recorded accelerograms as seismic input. IDA entails having each accelerogram in the ensemble scaled in amplitude to increasing levels of intensity (as measured by the selected IM) and estimating the structural response at each such level. In fact, because the IM typically does not possess full explanatory power with respect to structural response, the variability of the latter with respect to the former has to be captured. Thus, IDA seeks to map seismic structural response statistically, from the first signs of nonlinear inelastic behavior up to eventual collapse. Proposed extensions of this dynamic analysis methodology reserve the possibility of accounting for uncertainty in the numerical model itself (e.g., Dolsek, 2009, Vamvatsikos and Fragiadakis 2010, Vamvatsikos 2014). Alternative-to-IDA dynamic analysis strategies used for estimating structural fragility are *cloud analysis* and *multiple-stripe analysis* (e.g., Bazzuro et al., 1998, Jalayer and Cornell, 2003).

The main disadvantages of the dynamic-analysis-based derivation of fragility functions is the computational burden involved and the amount of effort that has to go into modelling highly non-linear structural behavior. The combination of numerical model complexity, required number of runs and the need for elaborate result post-processing can add-up to such demands of human and computing resources that engineers find themselves strongly motivated to look for simpler, approximate alternatives. The most notable simplifying alternative, one that has been with PBEE in various forms since its early years, involves making recourse to an equivalent single-degree of freedom (SDoF) inelastic system. One key point in this approximation is the assignment of a force-deformation law governing the SDoF system's response to monotonic lateral loading, typically referred to as the *backbone curve*. The definition of this backbone is typically based on the (numerically-evaluated) response of the original multiple-degree of freedom (MDoF) structure to a progressively increasing lateral force profile, known as its static push-over (SPO) curve. Due to their approximate nature, SPO-based methods have limitations that have been extensively documented and discussed (e.g., Krawinkler and Seneviratna, 1998; Fragiadakis et al., 2014).

The other key point that is ubiquitous among SPO-based procedures is the calculation of the seismic demand of the equivalent SDoF system and the subsequent estimation of the original MDoF structure's seismic demand (e.g., Fajfar, 2000). Throughout the years, semi-empirical methods available for this calculation have evolved from *the equal displacement rule* to equations relating strength ratio to ductility per oscillator period (often abbreviated as $R-\mu-T$ relations, e.g., Vidic et al., 1994) and eventually to the static pushover to IDA (SPO2IDA) algorithm of Vamvatsikos and Cornell (2006). While earlier inelastic-spectra-based approaches were focused on average response of SDoF oscillators with elastic-perfectly plastic or bilinear backbone curves, the more recent SPO2IDA tool has the ability to treat more complex SPO curves and, more importantly, offers direct estimates of the dispersion associated with the record-to-record variability of structural response. These two elements render SPO2IDA particularly suitable for implementation within the PBEE paradigm, since they facilitate the treatment of uncertainty in seismic structural response for limit states approaching global collapse.

This article comprehensively discusses the earthquake-engineering-oriented software SPO2FRAG (first introduced in Iervolino et al., 2016a), an application coded in MATLAB® environment that permits the computer-aided evaluation of seismic fragility functions for buildings, based on the results

of SPO analysis. The SPO2IDA algorithm lies at the core of SPO2FRAG, allowing the application to simulate the results of IDA without running numerous, cumbersome analyses.

The remainder of the paper is structured as follows: first, the background research behind SPO2FRAG is briefly presented, in order to highlight the connection between the PBEE paradigm and the program's functionality. The next section is dedicated to the detailed description of the program itself, addressing the various internal modules that comprise SPO2FRAG, the inner workings, methodology and flowchart, as well as the various options available to the user. Finally two illustrative examples are presented, along with some evaluation and discussion of the obtained results.

2. FRAGILITY, IDA, AND SPO2IDA

2.1 IDA and the IM-based approach

The conceptual basis of SPO2FRAG lies in simulating the results of incremental dynamic analysis using SPO alone. Therefore, the principal assumptions behind IDA and the methodologies for fitting analytical fragility models on IDA results are also relevant in this case and merit briefly recalling them.

IDA collects the responses of a non-linear structure to a suite of accelerograms, as these accelerograms are progressively scaled in amplitude to represent increasing levels of seismic intensity. These structural responses are typically represented by a scalar quantity, the engineering demand parameter (EDP). Examples of EDPs often used for buildings are maximum roof drift ratio (RDR) and maximum interstorey drift ratio over all floors (IDR). Furthermore, a scalar IM is chosen to represent seismic intensity; e.g., peak ground acceleration (PGA) or first-mode spectral acceleration, $Sa(T_1)$. One basic assumption is that such an IM is sufficient, that is, the EDP random variable conditioned on the IM is independent of other ground motion features needed to evaluate the seismic hazard for the site, such as magnitude and source-to-site distance. Another closely related assumption is the so-called *scaling robustness* of the chosen IM (e.g., Luco and Cornell, 2007), meaning that using records scaled to the desired amplitude of the IM, rather than records where said amplitude occurred naturally, will not introduce bias into the distribution of structural responses obtained (e.g., Iervolino and Cornell, 2005). This allows plotting EDP against IM as each individual record is scaled upwards, resulting in an IDA curve.

It is assumed that in the numerical model of the structure employed for IDA, stiffness and strength degradation under dynamic loading are acceptably represented. Consequently, failure of the analysis to provide an EDP value after scaling a record to a certain IM level can be attributed to the onset of dynamic instability, which would physically correspond to the structure's side-sway collapse (see also Adam and Ibarra, 2015). For presentation purposes, this numerical onset of collapse can be displayed at the end of the IDA curve as a horizontal segment of ever-increasing EDP-values for a fixed IM value, or a *flat-line* (see Figure 1). In cases where global collapse is deemed to occur at lower IMs due to non-simulated modes of failure (e.g., shear or axial failure of columns) an appropriate flatline may be used instead to terminate the IDA curve earlier.

An effective way of summarizing IDA results is to calculate and plot counted fractile curves of either EDP for fixed IM or vice-versa (Vamvatsikos and Cornell, 2004). Usually, fractile IDA curves at 16%, 50% and 84% are chosen for presentation, corresponding to the mean plus/minus one standard deviation of a Gaussian distribution. As a matter of fact, analytical derivation of fragility functions typically involves fitting a parametric probability model to the results of dynamic analysis and the

model chosen is very often lognormal. One way of defining the fragility function for a limit state is to assume that there exists a threshold (maximum allowable) value of some EDP, edp_f, whose exceedance also signals failure, i.e., exceedance of the limit state, according to Eq. (2).
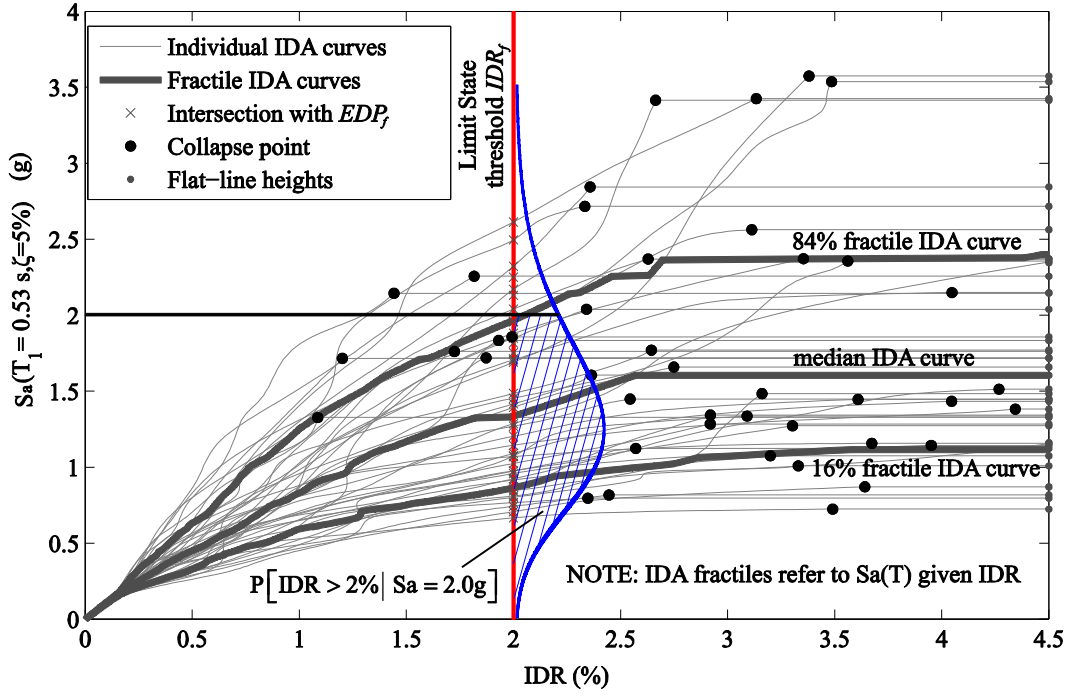

Figure 1. Example of IM-based derivation of structural fragility using IDA curves (limit state defined as exceedance of a 2% IDR value).

$$P\left[f \, | IM = im \right] = P\left[EDP > edp_f \, | IM = im \right] = P\left[IM_f^{LS} \leq im \right] \qquad (2)$$

An alternative way of looking at this fragility definition, within the IDA framework, can be stipulated by considering a random variable representing the IM level at which to scale a specific record in order to fail the structure (i.e., causing the event $EDP > edp_f$), denoted as IM_f^{LS}. In this case, the fragility function can be written as the probability of this random variable being equal or lower than the level of seismic intensity possibly occurring at the site, according to Eq. (2)– see also Jalayer and Cornell (2003). By making the assumption that IM_f^{LS} follows a lognormal distribution, the fragility function will be completely defined by estimating the two parameters of the underlying Gaussian, i.e., the mean of the logs η and the logarithmic standard deviation β. These parameters can be estimated using the sample of $IM_{f,i}^{LS}$ values shown in Figure 1 as the intersection of the individual IDA curves and the $EDP = edp_f$ vertical line. As a consequence, it is possible to write the fragility function via the standard Gaussian function $\Phi(\bullet)$:

$$P\left[IM_f^{LS} \leq im \right] = \Phi\left[\frac{\ln(im) - \eta}{\beta} \right] \qquad (3)$$

This approach, expressed by Eqs. (2)-(3), is known as the IM-based derivation of the fragility function. As evidenced in Figure 1, the IM-based approach is particularly convenient when global collapse becomes the limit state of interest: any vertical line intersecting all the records' flat-lines will provide the empirical distribution for collapse intensity to which a model such as the lognormal

appearing in Eq. (3) can be fitted. This, in turn, may be used to compute the failure rate via Eq. (1). In general, though, pinpointing a fixed value of edp_f that signals the transition between limit states can be hard due to the uncertainties involved.

It should be highlighted that when using IDA to estimate the fragility $P[f|IM = im]$ appearing in Eq. (1), the two already mentioned assumptions of sufficiency and robustness to scaling are endorsed by default, due to the very nature of the analysis. In what follows, it will be assumed that first mode spectral acceleration, $Sa(T_1)$, is a *sufficient-enough* IM with respect to roof and interstorey drifts for the structures considered and thus the problem of fragility estimation will be treated as site-independent.

2.2 Static pushover analysis and SPO2IDA

SPO analysis finds application in the context of earthquake engineering as part of several approximate procedures that relate the inelastic seismic response of structures to that of some equivalent SDoF system. The popularity of such methods can be attributed to their inherent simplicity and eventual adoption by normative documents and guidelines on seismic structural design/assessment. Some of the earlier examples of SPO-based procedures made recourse to elastic-perfectly plastic or bilinear SDoF equivalent oscillators and relied on inelastic displacement ratio predictive equations or $R - \mu - T$ (strength ratio – ductility – period) relations to obtain estimates of their average inelastic response. More recently, the trend has been shifting towards accounting for the variability of inelastic seismic response around its central value and towards expanding the limits of structural assessment to include global collapse (e.g., Vamvatsikos and Cornell, 2005). The latter of these trends practically translates into the adoption of more elaborate numerical models for the structure and consequently SPO curves that trace monotonic response to lateral loading down the (in-cycle) strength-degradation descending branch and along an eventual residual strength plateau. This, in turn, gives rise to the need for analytical models that predict the response of SDoF systems with more complex backbone curves, such as the quadrilinear depicted in Figure 2.
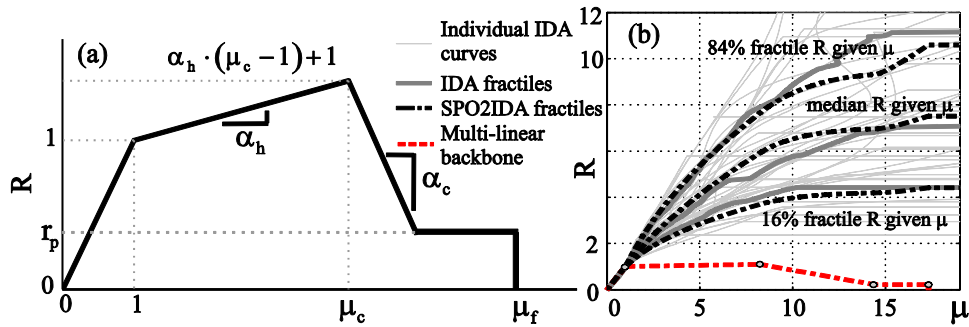

Figure 2. Quadrilinear monotonic backbone curve in dimensionless $\{R, \mu\}$ coordinates and defining parameters (a), SPO2IDA prediction against actual quadrilinear-backbone SDoF oscillator (T=0.56s) IDA curves obtained using all forty-four components of the FEMA P695 far-field ground motion set (b).

In this format, the quadrilinear backbone can be completely defined by five parameters shown in Figure 2(a): the hardening slope α_h (positive ratio of post-yield stiffness to elastic stiffness), the capping-point ductility μ_c (point where loss of strength with increasing deformation begins), the post-capping slope α_c (negative slope corresponding the ratio of the negative post-capping stiffness divided by the initial elastic stiffness), the height of the residual strength plateau r_p (ratio of residual

strength divided by yield strength) and the fracture ductility μ_f (point corresponding to sudden, complete loss of strength). It is recalled that ductility is defined as the ratio of displacement response to yield displacement, $\mu = \delta/\delta_y$, while the strength ratio $R = Sa(T)\big/Sa(T)_y$ is defined as the ratio of the spectral acceleration intensity to its value causing yield, or, equivalently, the ratio of the elastic seismic force over the yield base shear of the system (R is sometimes encountered in the literature under the term *strength reduction factor*).

Vamvatsikos and Cornell (2006) proposed a set of semi-empirical analytical equations aimed at predicting the median and (record-to-record) variability of peak seismic response of SDoF oscillators featuring quadrilinear SPOs. These equations use the SPO parameters α_h, μ_c, α_c, r_p, μ_f and period of natural vibration T as predictor (independent) variables to estimate the SDoF structure's 16%, 50% and 84% fractile IDA curves in $\{R,\mu\}$ coordinates. For this reason, this set of equations has been named SPO2IDA. The equations that comprise SPO2IDA were fit against the responses of SDoF oscillators with critical viscous damping ratios, ζ, equal to five percent and with hysteretic behavior exhibiting moderate pinching but no cyclic degradation of stiffness or strength. These oscillators were subjected to a suite of thirty recorded ground acceleration time-histories, recorded on firm soil and most likely unaffected by near-source directivity effects. An example of an SPO2IDA prediction for a quadrilinear-backbone SDoF system, plotted against the actual (individual and fractile) IDA responses for these thirty accelerograms, can be found in Figure 2(b). The limits of applicability for SPO2IDA in terms of the independent variables are the following: $0.10s \leq T \leq 4.0s$, $0.0 \leq \alpha_h \leq 0.90$,$1.0 < \mu_c \leq 9.0$, $0.02 \leq |\alpha_c| \leq 4.0$ and $0.0 \leq r_p \leq 0.95$.

The key observation behind the development of SPO2IDA was the relatively consistent behavior of the IDA fractile curves corresponding to the various segments of the underlying SPO (i.e., hardening, softening, residual). This behavior is visible in Figure 2(b), where the SPO is plotted along with the IDA fractiles (both calculated and predicted). While an almost-constant ascending slope characterizes the initial post-yield IDA segments, this gives way to gradual flattening upon crossing of the capping point. This flattening is temporarily arrested when the residual plateau is encountered, but only until the fracture point leads to the flat-lines that indicate collapse. Although analytically complex, SPO2IDA is an algorithm that has proven well-suited to computer implementation. SPO2FRAG fully exploits SPO2IDA's potential as a PBEE tool by surrounding it with a set of modules that render the SPO-based estimation of seismic structural fragility practical. The complete conceptual and operational details are presented in the following sections.

2.3 Definition of an equivalent SDoF system

The choice of an equivalent SDoF system for a given structure lies at the core of all SPO-based analysis methods. This choice entails the definition of the SDoF oscillator's mass, m^*, yield strength, F_y^*, yield displacement, δ_y^* and as many of the dimensionless backbone parameters (see Figure 2a) as are applicable to the case at hand (i.e., depending on whether one is opting for a bilinear, trilinear or full quadrilinear approximation of the SPO curve).
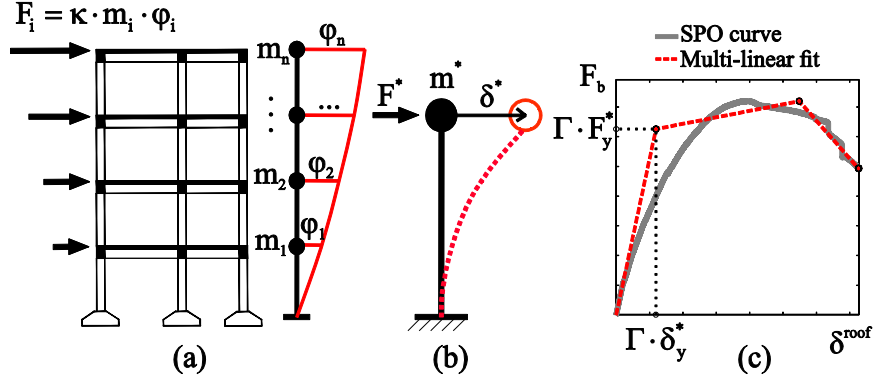
Figure 3. Definition of equivalent SDoF system: SPO analysis of the strtucture (a), definition of dynamic characteristics of the SDoF system (b), definition of monotonic backbone of the SDoF system based on SPO curve (c).

With reference to Figure 3, we assume that a generic n-storey frame building is subjected to a lateral load profile $F_i = \kappa \cdot m_i \cdot \varphi_i$, where F_i is the force acting on the i-th storey, m_i represents floor mass, the elements φ_i define a dimensionless displacement profile, which is assumed constant with unit value at roof level ($\varphi_n = 1$), and κ is a scale factor with dimensions of acceleration. By gradually increasing the scale factor κ , recording the displacement response of the deforming structure at roof level, δ^{roof} , and plotting that displacement against base shear, $F_b = \sum_{i=1}^{n} F_i$, we obtain the SPO curve - Figure 3(c). This curve is used to determine the monotonic backbone of an SDoF system whose mass, m^*, is given as a function of the structure's floor masses by $m^* = \sum_{i=1}^{n} m_i \cdot \varphi_i$ and whose reaction force F^* and displacement δ^* are related to the structure's base shear and roof displacement by dividing with the modal participation factor Γ ($F^* = F_b / \Gamma$ and $\delta^* = \delta^{roof} / \Gamma$) , which is calculated as $\Gamma = m^* \Big/ \sum_{i=1}^{n} m_i \cdot \varphi_i^2$ (Fajfar, 2000).

The period of vibration of the equivalent SDoF system, T^*, is calculated as $T^* = 2\pi \cdot \sqrt{\dfrac{m^* \cdot \delta_y^*}{F_y^*}}$. As indicated by Figure 3(c), the definition of F_y^* and δ_y^* depends on the piece-wise linear approximation adopted for the SPO curve. As far as specific methodologies towards obtaining said approximation are concerned, the literature offers some variety but little consensus. Normative documents such as Eurocode 8 (CEN, 2004), FEMA-356 (ASCE, 2000) and FEMA-273 (BSSC, 1997) suggest some procedures for obtaining elastic-perfectly-plastic or bilinear approximations for the backbone of the equivalent SDoF based on ad-hoc criteria such as *area balancing* (CEN, 2004). Furthermore, when it comes to trilinear or quadrilinear SPO fits that bring to the table a larger number of parameters to be estimated, such simple rules are not enough. In fact, more advanced methods towards constructing trilinear SPO curve approximations were proposed in FEMA-440 (2005), ASCE/SEI 41-06 (ASCE, 2007) as well as by Han et al. (2010) and Vamvatsikos and Cornell (2005).

Recently, De Luca et al. (2013) set forth a set of rules for obtaining quadrilinear approximations that may potentially include a residual strength plateau. In that work, the optimization of the piece-wise linear fit was performed by comparing the IDA curves of the multi-linear-backbone SDoF oscillator with those of the system sporting the exact backbone. For this reason, this was considered the most

suited algorithm for inclusion within SPO2FRAG's modules. In the aforementioned study, the authors paid particular attention to systems with SPOs exhibiting notable changes of stiffness already from the early, low-base-shear stages, e.g., Figure 3(c). Such a behavior, which can be due to, for example, gradual cracking of reinforced concrete (RC) members is especially challenging when it comes to pinpointing a nominal yield point for the equivalent SDoF system. It was concluded that the elastic segment of the equivalent system's backbone should correspond to a secant stiffness at an early point on the SPO curve, at around 5% to 10% of maximum base shear. This is due to the fact that when the elastic stiffness attributed to the equivalent system, F_y^*/δ_y^*, significantly departs from the initial tangent stiffness of the actual structure, the IDA curves corresponding to the linearized backbone display poor fit with respect to the IDAs of the *exact* backbone at the comparatively low-seismic-intensity region. This is especially relevant in cases where absence of a clearly defined elastic segment and high initial curvature characterizes the SPOs.

2.4 Consideration of MDoF effects

Once an equivalent SDoF oscillator has been fully determined, SPO2IDA can provide an approximation for the three fractile IDA curves of this SDoF system in $\{R, \mu\}$ coordinates, as already discussed (see Figure 4a). The predicted IDAs can be regarded as fractiles of strength ratio, $R_{x\%}$, given μ, with $x = \{16\%, 50\%, 84\%\}$. However, two further steps are needed before this result can be used to obtain a meaningful estimate for the fragility of the original MDoF structure. First of all, the SDoF IDA curves must be transformed from $\{R, \mu\}$ into an IM – EDP format appropriate for the structure. Second step is to address the variability of response at the nominal yield point $R = \mu = 1$. Prior to this point, the three IDA $R_{x\%}$ fractiles of the SDoF system coincide, corresponding to zero response variability around the median. On the other hand, the MDoF structure does exhibit response variability at that point. If the nominal yield point corresponds to the structure remaining in the elastic range, some limited variability will exist due to higher-mode contributions to base shear. Higher variability may be expected when the nominal yield corresponds to deformation levels where the structure is already manifesting some non-linear behavior (e.g., Figure 3c). In either case, the missing amount of variability should be estimated and injected back into the SDoF-derived approximation of the IDA curves. This is especially important when fragility for low-damage limit states is being sought. These operations are schematically presented in Figure 4b.
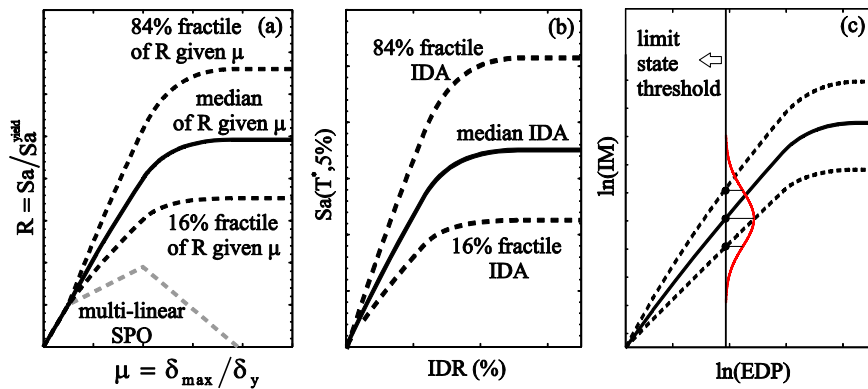

Figure 4. Schematic representation of the conceptual basis of SPO2FRAG: (a) obtaining SPO2IDA-predicted IDA fractiles for the equivalent SDoF system, (b) transforming the SDoF IDA curves to MDoF IM-EDP coordinates, (c) fitting Gaussian models to the transformed IDA fractiles according to the IM-based procedure (c).

Since the restoring force of the SDoF system depends on spectral acceleration at its natural period, T^*, the transformation of IM is the most immediate operation: the 16%, 50% and 84% fractiles of $Sa\left(T^*,5\%\right)$ are obtained from their counterpart R fractiles according to

$$Sa\left(T^*,5\%\right)_{x\%} = R_{x\%} \cdot \frac{\delta_y}{\Gamma} \cdot \left(\frac{2\pi}{T^*}\right)^2 \quad , x \in \{16,50,84\} \ .$$

The passage from ductility demand to RDR and IDR can be performed according to Eq. (4), where h_i denotes the height of the i-th storey and Γ_{eff} is an *effective* modal participation factor that can be used instead of Γ :

$$\begin{cases} RDR = \Gamma_{eff} \cdot \dfrac{\mu \cdot \delta_y^*}{\displaystyle\sum_{i=1}^{n} h_i} \\ IDR = COD \cdot RDR \end{cases} \tag{4}$$

In Eq. (4), the notation COD stands for *coefficient of distortion* (e.g., Moehle, 1992). COD is defined as the ratio of maximum IDR to the roof drift and is a function of R. This is expressed by Eq.(5), where δ_i represents the SPO displacement of the *i*-th storey at base shear level $R \cdot F_y$ and $H = \displaystyle\sum_{i=1}^{n} h_i$ the total building height:

$$COD = \frac{\max_i \left\{\left(\delta_i - \delta_{i-1}\right)/h_i\right\}}{\delta_n/H} \tag{5}$$

On the other hand, the effective modal participation factor Γ_{eff} appearing in Eq.(4) is intended to account for higher-mode effects and possible early (prior to nominal yield) non-linear behavior; for an example see Katsanos and Vamvatsikos (2017). Note that Γ_{eff} can be simply substituted by Γ when such effects are not of concern. In the context of SPO2FRAG, Γ_{eff} corresponds to an approximate analytical model that was developed using IDA results obtained for twenty-eight plane, steel and RC moment-resisting frames (MRFs) having two to eight storeys, first-mode periods within 0.25s-2.00s and using both distributed and concentrated plasticity models. The proposed functional form for Γ_{eff} is:

$$\begin{cases}
\Gamma_{eff} = \Gamma + R^2 \cdot \left(\sum_{i=1}^{n} m_i \Big/ \sum_{i=1}^{n} m_i \cdot \varphi_i - \Gamma \right) \cdot \left[\dfrac{Sa(T_2)}{Sa(T^*)} - 1 \right] \cdot \left[1 - 0.5 \cdot \left(\dfrac{T^*}{T_1} \right)^{1/2} \right] \ , \ 0 < R \le 1 \\[4mm]
\Gamma_{eff} = \Gamma + \left(\sum_{i=1}^{n} m_i \Big/ \sum_{i=1}^{n} m_i \cdot \varphi_i - \Gamma \right) \cdot \left[\dfrac{Sa(T_2)}{Sa(T^*)} - 1 \right] \times \\[4mm]
\quad \times \left[1 - 0.5 \cdot \left(\dfrac{T^*}{T_1} \right)^{1/2} - 1.7 \cdot \left(\dfrac{R-1}{R_{50\%}^{col}-1} \right)^{1/2} + 1.3 \cdot \left(\dfrac{R-1}{R_{50\%}^{col}-1} \right)^{1/2} \cdot \left(\dfrac{T^*}{T_1} \right)^{1/2} \right] \ , \ 1 < R \le R_{50\%}^{col} \\[4mm]
\Gamma_{eff} = \Gamma + \left(\sum_{i=1}^{n} m_i \Big/ \sum_{i=1}^{n} m_i \cdot \varphi_i - \Gamma \right) \cdot \left[\dfrac{\widetilde{Sa(T_2)}}{Sa(T^*)} - 1 \right] \cdot \left[0.8 \cdot \left(\dfrac{T^*}{T_1} \right)^{1/2} - 0.7 \right] \ , \ R > R_{50\%}^{col} \\[6mm]
1.0 \le \left(T^*/T_1 \right)^{1/2} \le 1.50, \ 1.0 \le \widetilde{Sa(T_2)} \Big/ Sa(T^*) \le 3.0
\end{cases} \qquad (6)$$

In Eq. (6), $Sa(T_2)$ represents the geometric mean spectral acceleration at the second-mode period, when all records of the ground motion suite employed by Vamvatsikos and Cornell (2006) for SPO2IDA are scaled to a common $Sa(T^*)$ value. On the other hand, $R_{50\%}^{col}$ represents the median strength ratio causing collapse, taken as the median SPO2IDA flat-line height.

Note that according to Eq.(6), Γ_{eff} can assume values between Γ (lower bound) and $\sum_{i=1}^{n} m_i \Big/ \sum_{i=1}^{n} m_i \cdot \varphi_i$ (upper bound). The upper bound value corresponds to activation of the full structural mass along the vibration mode φ_i. Furthermore, Γ_{eff} depends on R, T^*/T_1, and $Sa(T_2) \Big/ Sa(T^*)$. The ratio T^*/T_1 is a measure of how far the nominal yield point of the equivalent SDoF system trespasses into non-linear territory; higher values of this ratio correspond to SPO curves with considerable initial curvature. The ratio $Sa(T_2) \Big/ Sa(T^*)$ is in place to account for the response-amplifying effect of higher modes, when the structure is excited by accelerograms exhibiting larger spectral ordinates at the second-mode period. It has been known for some time that, in MRF structures, such effects persist into the non-linear response range (e.g., Shome and Cornell, 1999).

The second part of the SDoF to MDoF transition consists of adding the missing variability at nominal yield, β_y. Vamvatsikos and Cornell (2005) suggested that this can be achieved by running a set of linear-elastic response history analyses of the structure. Although that approach may work when nominal yield of the equivalent SDoF system coincides with the linear-elastic limit of the structure, in order to deal with a generic case when the former delves into non-linear territory a semi-empirical relation was developed for the purposes of SPO2FRAG. This relation was calibrated using the same stock of buildings' numerical models as for Eq. (6):

$$\begin{cases} \beta_y = \sqrt{\beta_{yo}^2 + \beta_{y,T_2}^2} \\[2mm] \beta_{yo} = 1/2 \cdot \ln\left(Sa_{y,84\%}^{bilin} \middle/ Sa_{y,16\%}^{bilin} \right) \\[2mm] \beta_{y,T_2} = 0.04 + 0.04 \cdot \dfrac{Sa(T_2)}{Sa(T^*)} \cdot \left[2.6 - 1.6 \cdot \left(\dfrac{T_{sec}}{T_1} \right)^{1/2} \right] \\[3mm] T_{sec} = 2\pi \cdot \sqrt{\dfrac{m^* \cdot \delta_y}{F_y}}, \;\; 1.0 \le \left(T_{sec}/T_1 \right)^{1/2} \le 1.5 \end{cases} \tag{7}$$

According to Eq. (7), two separate contributions are considered in the estimate of β_y. The term β_{yo} that accounts for early non-linear behavior (i.e., curvature of the SPO curve prior to the nominal yield point) and the term β_{y,T_2} that accounts for purely higher-mode contribution to variability at yield. The other terms introduced in Eq. (7) are the secant-to-first-mode period ratio T_{sec}/T_1 and the $Sa_{y,x\%}^{bilin}$ fractiles that determine β_{yo}. The terms $Sa_{y,x\%}^{bilin}$ appearing in Eq. (7), correspond to the x% SPO2IDA fractiles of an auxiliary SDoF system, whose bilinear backbone is fitted using only the SPO segment that precedes the nominal yield point; this means that β_{yo} attains higher values as the nominal yield point advances into the non-linear part of the SPO curve and reduces to zero whenever nominal yield is found on the initial linear segment. The T_{sec}/T_1 ratio used in the calculation of the β_{y,T_2} term is another proxy for early SPO curvature; note that according to Eq.(7), the influence of the higher-mode term β_{y,T_2} diminishes for increasing values of T_{sec}/T_1. This is explained by the fact that larger values of T_{sec}/T_1 imply substantial initial curvature of the SPO curve, in which case the competing term β_{yo} tends to account for most of the variability. It should be noted that the combination of employing the Γ_{eff} concept and injecting the missing variability at yield β_y, constitutes a simplified method of dealing with higher-mode effects in the context of SPO analysis that was tailor-made to suit the needs of the SPO2FRAG software; therefore, caution is advised should it be used to confront this complex issue outside this context.

2.5 SPO-based fragility

Having thus simulated the three IDA fractile curves, based on the SPO of the structure, the parameters of the lognormal fragility model of Eq. (3) can be fitted for each limit-state (Figure 4c). Since the SPO-based IDA approximation does not provide the individual IDA curves, but only fractiles, the fragility parameters can be estimated as:

$$\begin{cases} \eta = \ln\left(Sa_{f,50\%}^{LS} \right) \\[2mm] \beta = \ln\left(Sa_{f,50\%}^{LS} \middle/ Sa_{f,16\%}^{LS} \right) \end{cases} \tag{8}$$

The terms $Sa_{f,x\%}^{LS}$ represent the x% fractile of the structural intensity causing exceedance of each limit state LS, as defined when introducing Eq. (2) and IM-based fragility.

Finally, once the lognormal fragility parameters $\{\eta, \beta\}$ have been estimated from the SPO analysis one may consider two a posteriori modifications. One modification to the median, in order to account for structural damping other than $\zeta = 5\%$ and another modification to the dispersion that accounts

for additional response variability due to structural modelling uncertainty. In the $\zeta \neq 5\%$ case, it is considered that it is sufficient to modify the median and only for limit states nearing collapse. In fact, Han et al. (2010) proposed a modification factor, C_ζ, to be applied to the median collapse intensity of 5%-damped SDoF systems:

$$\begin{cases} R_{50\%}^{col}(\zeta) = C_\zeta \cdot R_{50\%}^{col}(\zeta = 5\%) \\ C_\zeta = 1 - \dfrac{0.07 \cdot \ln \zeta + 0.20}{\left(T^*\right)^{0.38} \cdot \left|\alpha_c\right|^{-0.26} \cdot \mu_c^{-0.44}} \end{cases} \qquad (9)$$

However, even for structures with $\zeta \neq 5\%$, it is desirable to maintain $Sa\left(T^*, 5\%\right)$ as IM, since hazard is typically available in terms of 5%-damped spectral ordinates. Therefore, the necessary modification boils down to Eq. (10), where η_ζ^{col} represents the logarithmic mean collapsing intensity of a $\zeta \neq 5\%$ structure in terms of $Sa\left(T^*, 5\%\right)$ and $\eta_{\zeta=5\%}^{col}$ is the uncorrected SPO2IDA estimate from Eq. (8), that considers $\zeta = 5\%$ by default:

$$\eta_\zeta^{col} = \eta_{\zeta=5\%}^{col} - \ln C_\zeta \qquad (10)$$

Apart from the modification of Eq. (10), which is applicable at collapse, a modification factor is also applied to the median failure intensity of any limit states defined by EDP thresholds in proximity to collapse. These modification factors are obtained by interpolation, based on the requisite that η increase monotonically with edp_f.

When a single deterministic numerical model of the structure is subjected to IDA, the distribution of the obtained responses reflects record-to-record variability. However, one may also wish to account for uncertainty underlying the mechanical model parameters (such as material strength, member hysteretic behavior, mass distribution, etc.). A simple method for dealing with this issue, adopted by Cornell et al. (2002), is the so-called first-order assumption, whereby the mean logarithmic failure intensity is itself a normal random variable, depending on the probabilistic configuration of the structural model, with a standard deviation β_U and mean η. Then, the fragility function remains lognormal with the same mean, but with variance $\beta_{tot}^2 = \beta^2 + \beta_U^2$, with β representing response variability estimated directly from SPO2IDA and Eq. (8). The variability due to modelling uncertainty, β_U, can either directly assume a value proposed in the literature (e.g., values suggested in FEMA P-695 for the collapse limit state) or be estimated by combining SPO2IDA and Monte-Carlo simulation, similar to what was suggested by Fragiadakis and Vamvatsikos (2010), to follow.

3. OPERATIONAL OUTLINE OF SPO2FRAG

The SPO2FRAG tool is essentially a software implementation of the methodology for the SPO-based derivation of seismic fragility functions presented in detail in the preceding section. This engineering application revolves around a graphical user interface (GUI), which is divided in three parts (Figure 5): the SPO to IDA and fragility toolboxes, panels for the visualization of intermediate results (SPO processing and IDA curve generation) and an output panel where the end result in the form of fragility curves is visualized.
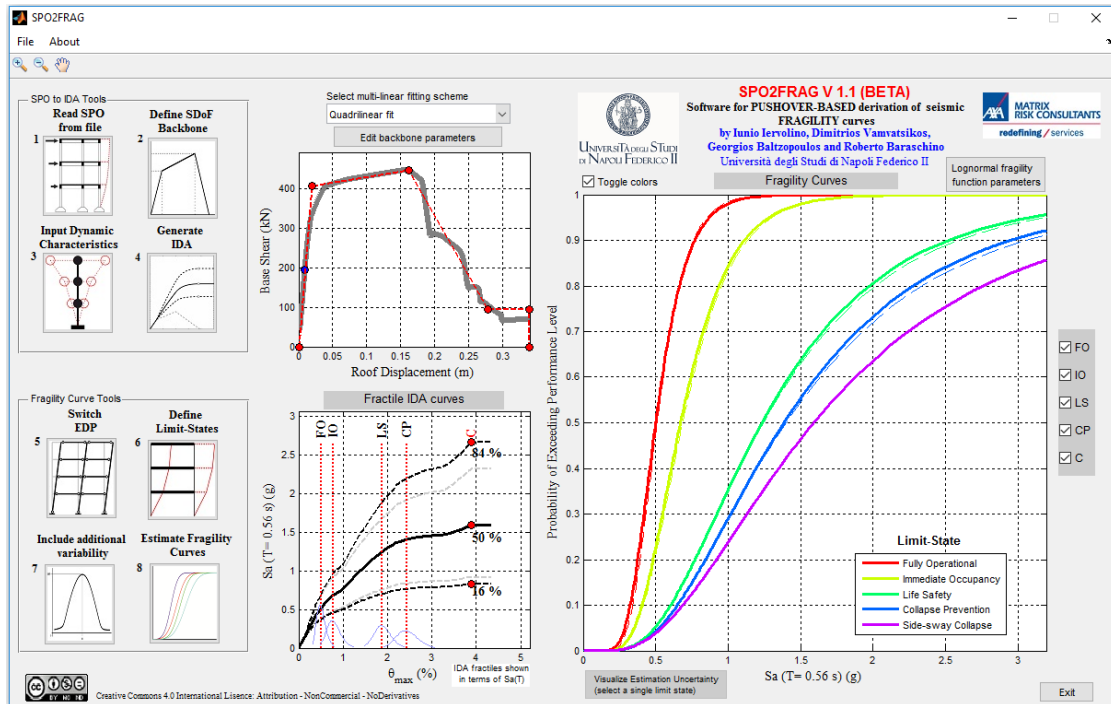
Figure 5. Main SPO2FRAG GUI displaying a completed elaboration of fragility curve calculation.

In operational terms, SPO2FRAG comprises a series of individual modules that function independently and complement one another:

1. input interface;
2. automatic multi-linearization tool;
3. dynamic characteristics interface;
4. SPO2IDA module;
5. EDP conversion tool;
6. limit-state definition interface;
7. additional variability management tool;
8. fragility parameter-fitting module.

These modules are organized into two toolboxes on the main GUI and operate according to the flowchart of Figure 6.
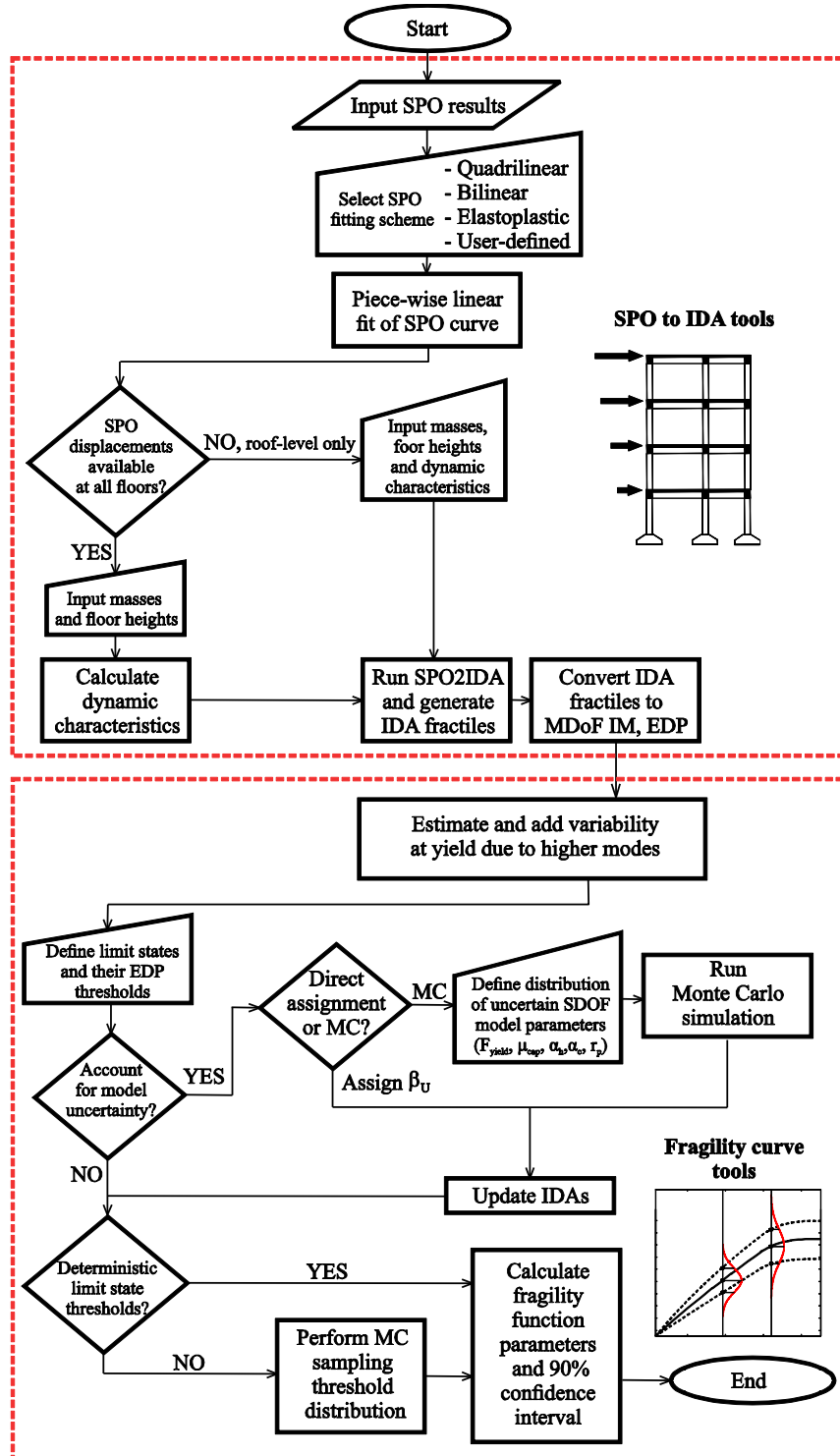
Figure 6. SPO2FRAG flowchart, schematically showing the grouping of the sub-modules into "SPO2IDA tools" and "Fragility curve tools".

3.1 Data input and definition of equivalent SDoF system

The SPO2FRAG tool does not include structural analysis code and operates on the premise that the necessary static non-linear and any optional modal analysis are performed externally. Therefore, any SPO2FRAG project starts at the data input interface, which reads SPO force-displacement results from either a text or a spreadsheet file.

The user is advised to provide SPO displacements at all storeys (rather than just at roof level) since this lateral deformation profile δ_i can then be used by the program to compute the COD according to Eq.(5), permitting a direct SPO-based conversion of RDR to IDR – Eq. (4). During input, the SPO curve is subjected to some rudimentary checks for correctness and consistency. Subsequently, the roof displacement – base shear values are forwarded to the automated piece-wise linear fitting module.
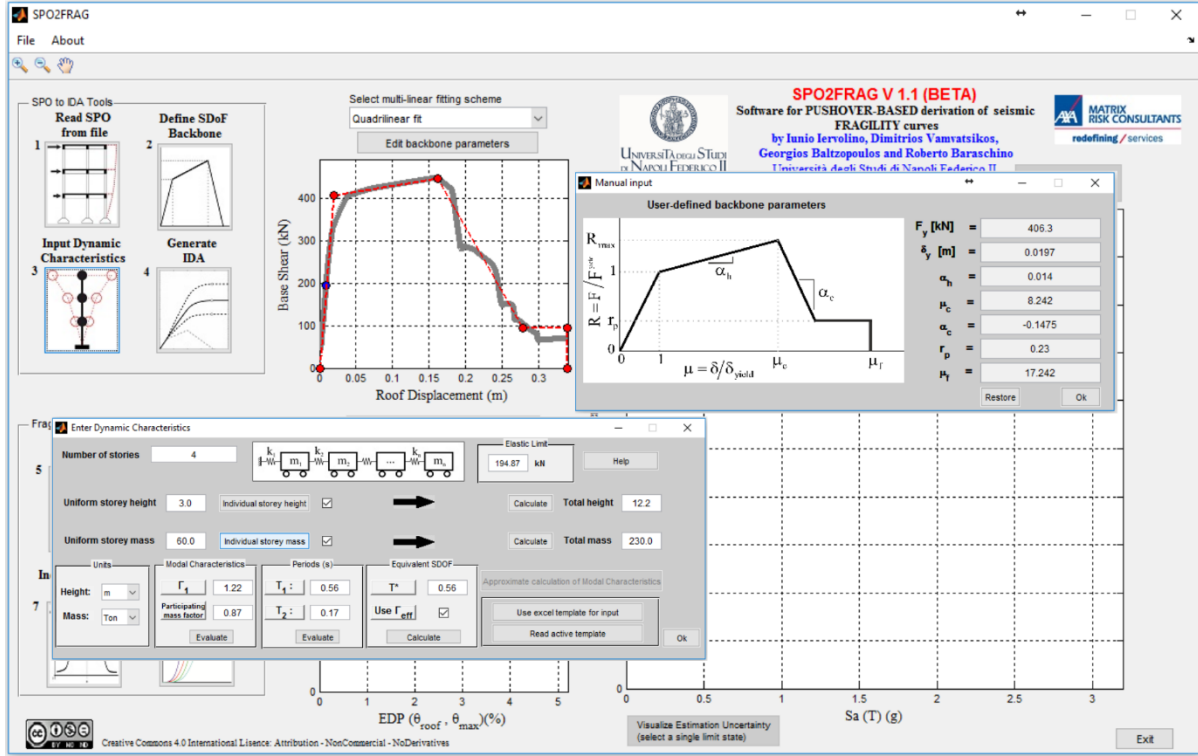

Figure 7. Multi-linear backbone definition for the equivalent SDoF system and input of dynamic and geometric characteristics of the MDoF structure (spring-mass representation is purely indicative) within the SPO2FRAG GUI.

The multi-linear fit module is intended to aid the user in the definition of the equivalent SDoF backbone curve and allows for the options listed below:

- *quadrilinear fit*; the SDoF backbone curve receives a piece-wise linear fit based on the work of De Luca et al. (2013), potentially comprising a maximum of four segments: elastic, hardening, softening and residual strength. Corresponding parameter values are determined via a Monte-Carlo-based optimization algorithm.
- *bilinear fit*; two-segment (elastic-hardening) fit in the spirit of the FEMA-356 displacement coefficient method (FEMA, 2000), again according to criteria set forth by De Luca et al. (2013).
- *elastic-perfectly plastic fit*; simple bilinear elastoplastic fit based on area balancing, compatible with code prescriptions (e.g., EN 1998-1, 2004), ending when strength drops below 80% of maximum (or at the last available SPO point).
- *user-defined backbone parameters*: manual input by the user.

The multitude of fitting-scheme choices is intended to accommodate various levels of refinement in the numerical modelling, at the user's discretion. The user is also given the option to intervene and override any of the automatically assigned backbone parameters.

Once the backbone parameters have been established, data input continues with the dynamic characteristics and geometric configuration of the structure (Figure 7). Additional data required at

15

this stage consist of floor masses and storey heights, the first and second mode vibration periods and the participating mass factor. In cases where the user has provided SPO displacement values at all storeys, SPO2FRAG offers the option of internally approximating the modal participation factor, participating mass and first-mode period. First of all, a segment of the SPO curve is sought that corresponds to linear-elastic response (within a certain tolerance). The force (base shear) and i-th floor displacement values at the end of said segment are denoted as F_{el} and $\delta_{el,i}$, $i = \{1,...,n\}$ with n corresponding to the top-most storey, as per the convention of Figure 3. By making the assumption that the lateral force profile sufficiently approximates the first modal load vector, Γ, T_1 and the participating mass, $\tilde{m}$, can be automatically estimated by the program according to Eq. (11).

$$
\begin{cases}
\Gamma \approx \delta_{el,\mathrm{n}} \cdot \left(\sum_{i=1}^{n} m_i \cdot \delta_{el,i} \right) \Big/ \left(\sum_{i=1}^{n} m_i \cdot \delta_{el,i}^2 \right) \\[4mm]
\tilde{m} \approx \dfrac{\left(\sum_{i=1}^{n} m_i \cdot \delta_{el,i} \right)^2}{\sum_{i=1}^{n} m_i \cdot \delta_{el,i}^2 \cdot \sum_{i=1}^{n} m_i} \\[4mm]
T_1 \approx 2\pi \cdot \sqrt{ F_{el} \Big/ \left(\sum_{i=1}^{n} m_i \cdot \delta_{el,i} \right) }
\end{cases}
\tag{11}
$$

This is also the point where the user is called upon to decide whether to opt for the SDoF to MDoF EDP conversions using Γ_{eff} as per Eq. (6) or to simply set $\Gamma = \Gamma_{eff}$. The former choice can add accuracy to the approximation for structures with non-negligible higher-mode contribution to the response, while the latter is a cautionary choice for cases when the user desires to employ some particular backbone fit of his own devising.

3.2 The SPO2IDA module and SDoF to MDoF conversions

Once the data input and multi-linear fit of the SPO curve phases have been concluded, the SPO2IDA module is activated, providing the approximated 16%, 50% and 84% IDA fractile curves in $\{R, \mu\}$ terms. This SPO2IDA output is internally converted into $Sa(T^*, 5\%)$ versus drift coordinates. In cases where the SPO displacements at all storeys have been provided, the default is to convert the IDAs into IDR with the aid of Eq.(5) ; otherwise, RDR is employed, as estimated via Eq. (4). In the latter case, the user is still given the option to switch to IDR, using the approximate equations for the lateral post-yield deformation profile suggested in FEMA P-58-1 (FEMA, 2012).

3.3 Definition of performance limit states

By default, SPO2FRAG recognizes five seismic performance limit states, but the user is given the choice to add or remove limit states for each project. The first four limit states are labeled *fully operational*, *immediate occupancy*, *life safety* and *collapse prevention* (see SEAOC, 1995 or FEMA, 2000 for definitions). The fifth limit state, labeled *side-sway collapse*, is added by SPO2FRAG when the SPO curve exhibits strength degradation in the form of a negative-stiffness branch. This limit state corresponds to dynamic instability and is matched to the IDA flat-lines, without requesting any further user-input. The user may also opt to introduce any non-simulated collapse modes by appropriately truncating the SPO curve, whereby this limit-state (and the corresponding flatlines) more reliably indicate the occurrence of global collapse. For the remainder of the limit states, the user is expected

to define thresholds in terms of EDP that determine each one's exceedance. Exceedance thresholds may be inserted explicitly or defined on the SPO curve (e.g., at specified values of global ductility or percentage of peak strength loss), via a dedicated tool contained in the limit-state module (Figure 8). An additional option available to the user is to treat some or all of these exceedance thresholds as random variables by assuming that they follow a lognormal distribution. In this case, the threshold EDP value is taken as the median value and the user must define the log-standard deviation as well.
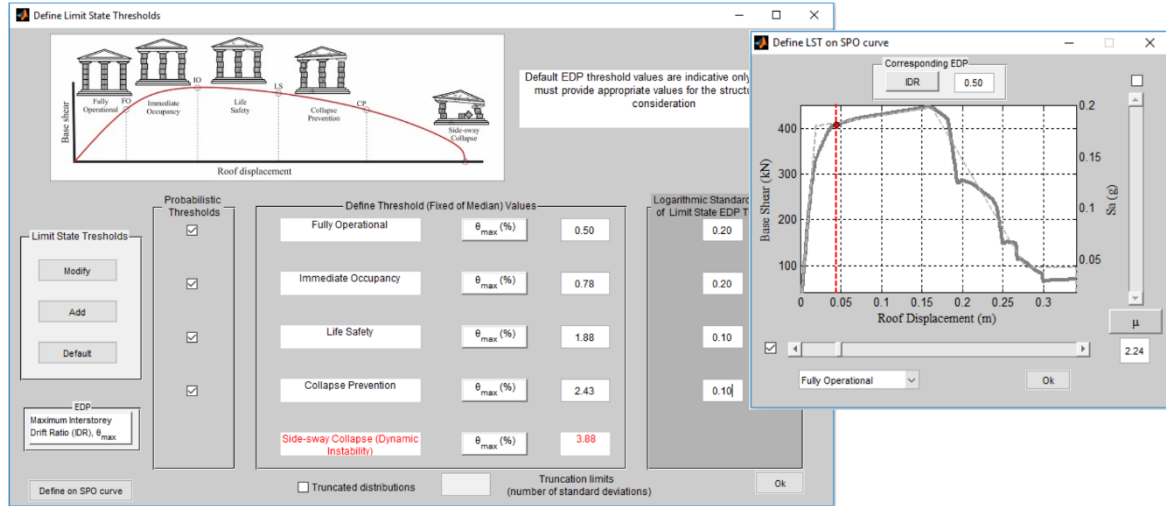

Figure 8. Limit-state threshold definition window and subsidiary tool for operating on the SPO curve while defining the thresholds.

3.4 Managing additional sources of variability

At this point, even though SPO2FRAG has accumulated sufficient information to be able to proceed with the estimation of the fragility function parameters according to Eq. (8), two issues pertaining to the introduction of additional response variability remain to be addressed on an optional basis. The first of these issues is the fact that, prior to nominal yield, the MDoF system exhibits record-to-record variability that has not yet been accounted for in the SDoF to MDoF transformation, resulting in the 16% and 84% IDA fractiles temporarily coinciding with the median for drift values corresponding to $R \leq 1$. This shortcoming can be remedied at this juncture by injecting an estimate for this missing variability at nominal yield, which is then propagated along the IDA 16% and 84% fractiles. Users may employ the values automatically provided by SPO2FRAG, according to Eq. (7), or override them with their own values from external analysis (e.g., as suggested by Vamvatsikos and Cornell, 2005). This addition can be important when the fragilities of high-performance limit states are of interest (i.e., those corresponding to practically unscathed post-earthquake functionality of the building).

The second optional issue concerns cases where one wishes to account for model uncertainty in the fragility curves. This translates to additional response variability, which can be incorporated into the approximated SPO2FRAG IDA curves by symmetrically (in log-space) distancing the 16% and 84% fractiles away from the median. This only leaves the parameter β_U to be determined for each limit state and the corresponding SPO2FRAG module offers two options for doing so (Figure 9). The first option entails user-definition of a β_U value at one of the predetermined limit states. This value could be obtained from the technical literature and should be appropriate for the structure and the level of modeling sophistication at hand. This additional uncertainty is then propagated along the IDA curves in a manner that ensures their monotonicity.
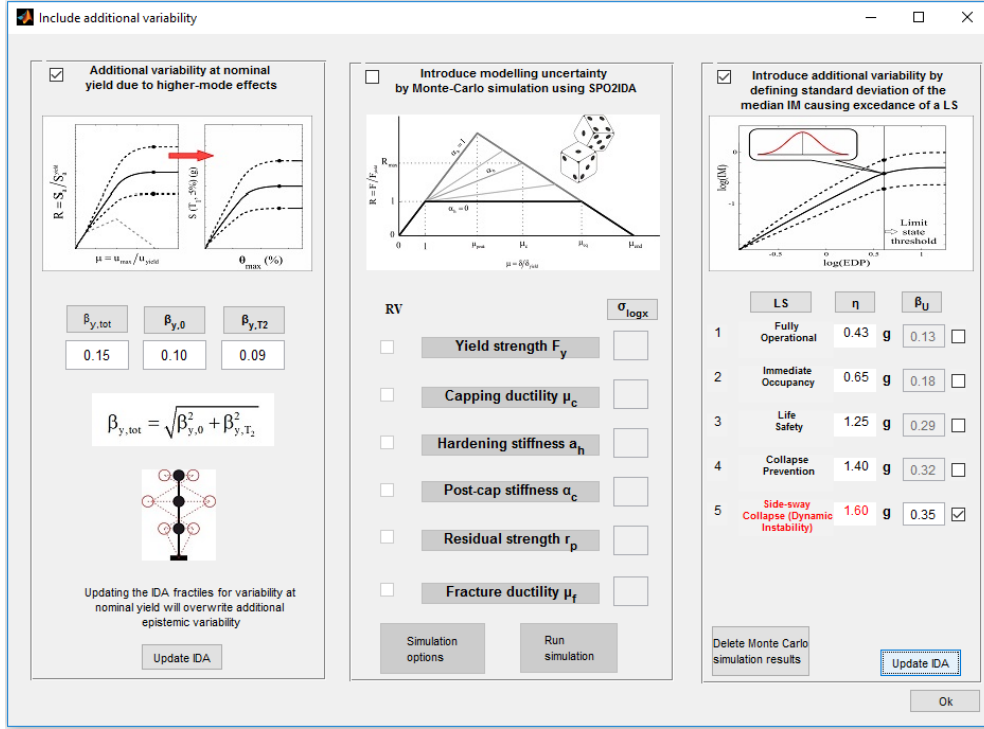
Figure 9. SPO2FRAG's window for the additional variability management module.

The second option is to estimate β_U via a combination of SPO2IDA and Monte Carlo simulation. In this second case, some of the parameters that define the equivalent SDoF backbone are treated as lognormally distributed, independent random variables, whose variance is determined by the user (the median is taken by default as the value defining the current equivalent SDoF backbone). According to this methodology, a number of M Monte Carlo realizations of the backbone are created by sampling from these distributions and subsequently SPO2IDA is used to obtain the median intensity per limit state exceedance for the j-th backbone realization, $\left(Sa_{f,50\%}^{LS}\right)_j$, $j=\{1,...,M\}$. Then, β_U can be estimated according to Eq. (12).

$$\beta_U = \sqrt{\frac{1}{M-1} \cdot \sum_{j=1}^{M}\left[\ln\left(Sa_{f,50\%}^{LS}\right)_j - \frac{1}{M} \cdot \sum_{i=1}^{M}\ln\left(Sa_{f,50\%}^{LS}\right)_i\right]^2} \qquad (12)$$

This operation follows the spirit of the methodology of Fragiadakis and Vamvatsikos (2010), the difference being that, in this case, the Monte Carlo simulations are performed by sampling directly the piece-wise linear equivalent SDoF backbones, rather than by executing new SPO analysis runs.

3.5 Fragility curve parameters

Upon the conclusion of the preceding operations (even without consideration of additional uncertainty) the fragility function estimation module may be activated. At this point, SPO2FRAG will query the user regarding the damping ratio ζ characterizing the structure and the choice of estimator for the dispersion parameter (see also Figure 10). The former information is needed whenever a correction for $\zeta \neq 5\%$ should be applied to the estimated logarithmic mean according to Eq. (10), while the latter provides an alternative to the estimation of β given in Eq. (8): Instead of using the log-space distance between the 50th and the 16th percentile failure intensities, one may opt

to use instead the log-space half-distance between the 84th and 16th percentiles, $\beta = 1/2 \cdot \ln \left(Sa_{f,84\%}^{LS} / Sa_{f,16\%}^{LS} \right)$.

SPO2FRAG uses Eq. (8) by default for two reasons. If one selects, among alternative SPO lateral force profiles, the one that leads to the earliest failure of the structure (as recommended by Vamvatsikos and Cornell, 2005) the SPO-based backbone will correspond to that single collapse mechanism. On the other hand, IDA of the MDoF structure will reveal a variety of collapse mechanisms for different records – see for example Haselton et al. (2011). Recognizing that the IDA curves corresponding to the more favorable collapse mechanisms should be more influential towards the shape of the 84% failure intensity fractile, it is to be equally expected that the more unfavorable (e.g., soft-storey mechanisms) similarly dominate the 16% fractile. Hence, one concludes that choosing the most unfavorable SPO lateral load profile could result in the lower (50% and 16%) fractile curves being better approximated through SPO2IDA than the 84% one. The second reason is that Eq. (8) may be regarded as compatible with a *truncated IDA* analysis strategy (e.g., Baker, 2015), where an analyst chooses to run IDA but only scale records up to a certain IM level (e.g., until 50% of records induce collapse). This truncated IDA scheme may be dictated by the desire to avoid any scaling bias that might lurk above the considered IM limit (see for example Kwong et al., 2015).
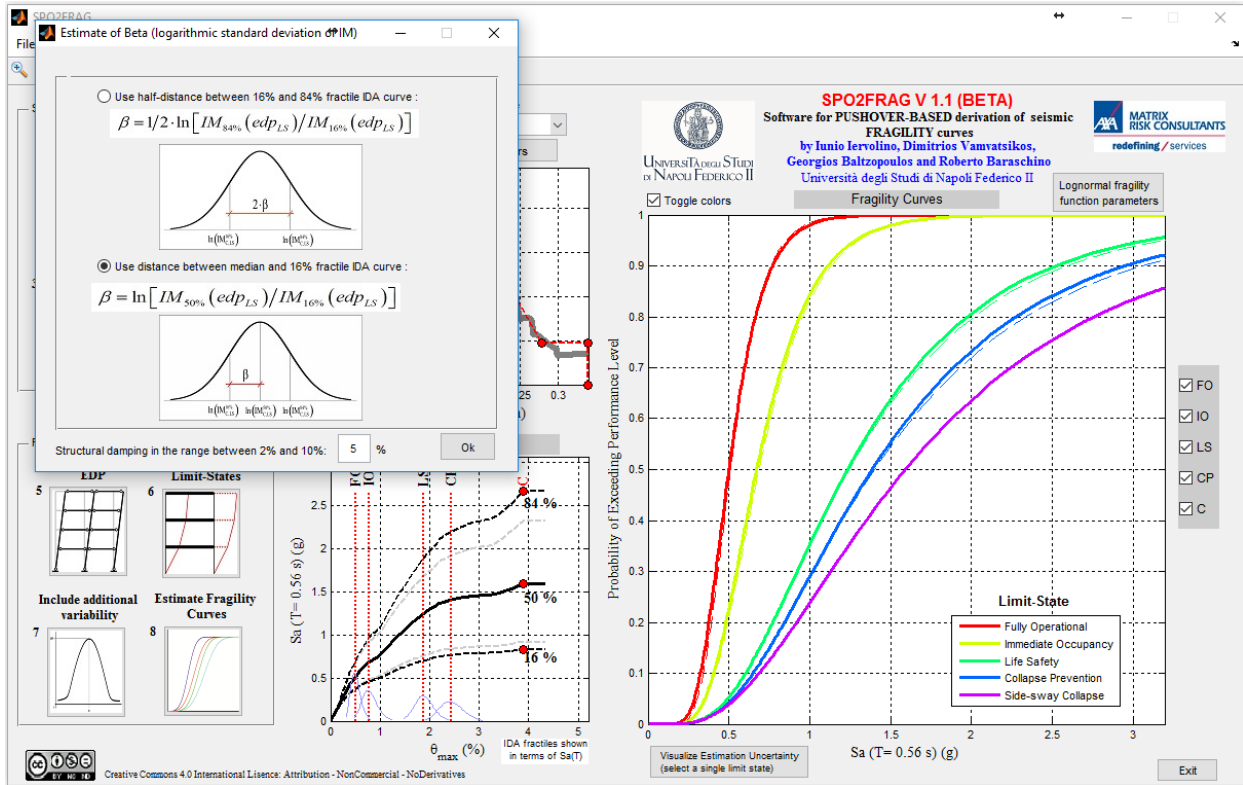

Figure 10. SPO2FRAG's dialogue window upon activation of the fragility-function estimation module.

For all limit states that have been assigned deterministic exceedance thresholds, estimation of the lognormal fragility function parameters $\{\eta, \beta\}$ proceeds as described in detail in paragraph 2.5. In cases where some limit states have been assigned exceedance thresholds with an associated lognormal probability density, the fragility function is estimated by means of numerically evaluating, via Monte Carlo, the integral resulting from application of the total probability theorem:

$$P\left[IM_f^{LS} \le im\right] = \int_{EDP_f} \Phi\left[\frac{\ln(im) - \eta_{edp_f}}{\beta_{edp_f}}\right] \cdot f_{EDP_f}\left(edp_f\right) \cdot d\left(edp_f\right) \quad (13)$$

In Eq. (13), $f_{EDP_f}\left(edp_f\right)$ is the probability density function of EDP_f and η_{edp_f}, β_{edp_f} are the logarithmic mean and standard deviation of IM_f^{LS} conditional on the limit state threshold assuming each specific value $EDP = edp_f$. A noteworthy result of normal theory applicable in this case is that, when $f_{EDP_f}\left(edp_f\right)$ is a lognormal density, then $P\left[IM_f^{LS} \le im\right]$, as given by Eq. (13), also follows the lognormal model.
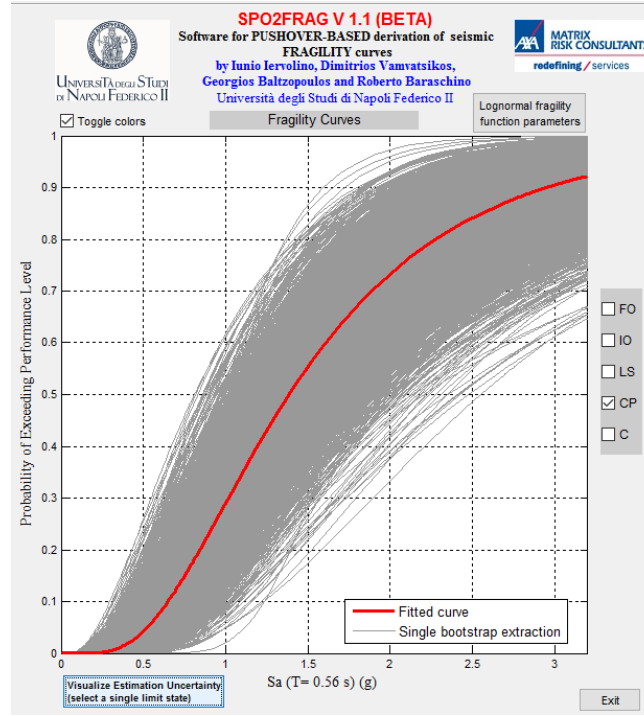

Figure 11. Visualization of estimation uncertainty underlying the fragility parameter estimates with the aid of a parametric-bootstrap-generated set of alternative fragility curves.

3.6 Consideration of estimation uncertainty

The SPO2FRAG tool estimates seismic fragility according to the IM-based procedure described in paragraph 2.1, by simulating dynamic analysis results via the SPO2IDA algorithm. Since the SPO2IDA equations were fit against IDA responses to a suite of thirty recorded accelerograms (Vamvatsikos and Cornell, 2006), the fragility parameter estimates provided by SPO2FRAG can be implicitly regarded as (fixed-size) sample estimators of a Gaussian model's parameters. As such, the estimators for the mean and variance are probabilistic results that are affected by uncertainty of estimation, i.e., the uncertainty inherent in estimating the mean and variance of a population based on an extracted finite-size sample (Mood, 1974).

Since quantification of estimation uncertainty associated with structural fragility may be of interest for the seismic risk analyst, SPO2FRAG calculates the boundaries of the 90% confidence interval for each limit state's parameter estimates. Furthermore, SPO2FRAG also provides the user with a visual representation of the estimation uncertainty associated with the fragility curves obtained, shown in Figure 11. The plot depicted is generated using parametric bootstrap (Efron, 1982). The parametric bootstrap belongs to a family of resampling schemes for the approximate calculation of estimator

statistics and is simulation-based. In the case at hand, a fixed number of twenty-five hundred bootstrap samples of size thirty are extracted from the Gaussian distribution defined by the SPO2FRAG-estimated fragility parameters. Then, a new pair of lognormal fragility parameters is re-estimated for each extraction. Finally, the fragility functions corresponding to each bootstrap extraction are plotted against the originally fitted fragility curve, resulting in Figure 11.

4. ILLUSTRATIVE SPO2FRAG APPLICATIONS

In order to be able to illustrate SPO2FRAG's function and compare the resulting fragility functions with their dynamic-analysis-derived counterparts, two applications on MRFs are presented where seismic fragility functions are obtained both by means of SPO2FRAG and via IDA.

4.1 Structures, numerical models and set of ground motions used in the analyses

The two case-study structures used in these examples are a four-storey steel MRF and a six-storey RC-MRF. The four-storey steel MRF (Figure 12a) belongs to a set of archetype structures designed and employed for the purposes of the NIST GCR 10-917-8 report (NIST, 2010). On the other hand, the six-storey RC-MRF (Figure 12c) was designed and used by Baltzopoulos et al. (2015), where information on member detailing can be found.
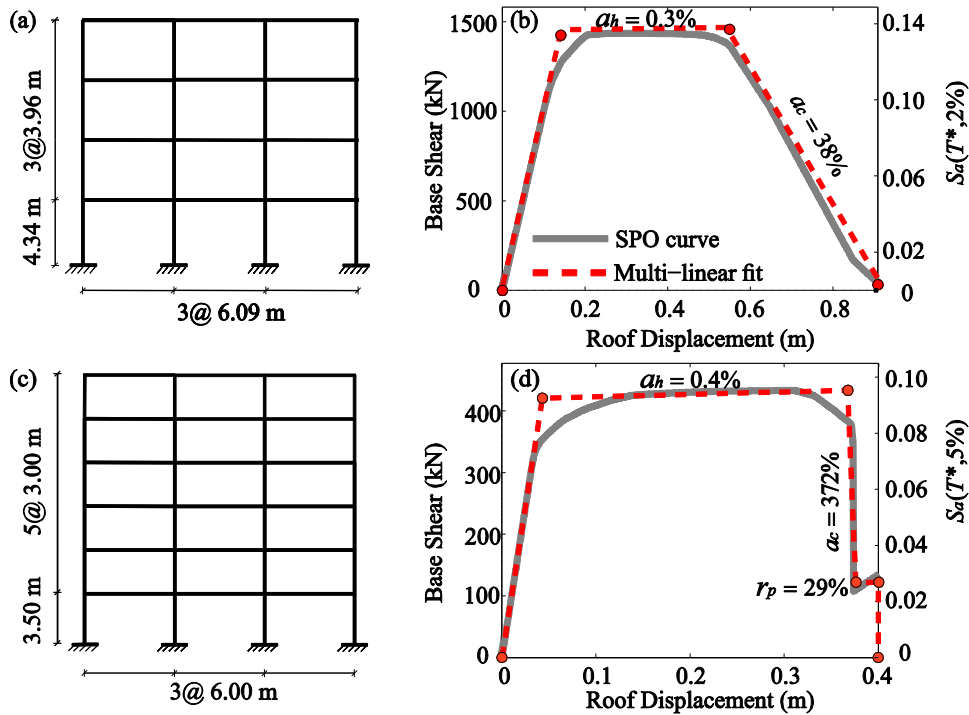

Figure 12. Geometry of centerline idealizations of the two MRFs and corresponding SPO curves. Four-storey steel MRF geometry (a) and SPO (b). Six-storey RC-MRF geometry (c) and SPO (d).

Both frames were modelled numerically using 2D centerline finite element representations in the OpenSEES structural analysis platform (McKenna et al., 2000). Material non-linearity was accounted for using a concentrated plasticity approach. The properties of the monotonic backbone of the plastic hinges at member edges were estimated using the regression equations suggested by Lignos and Krawinkler (2011) for the steel and those by Haselton and Deierlein (2007) for the RC frame, while a moderately pinching hysteretic law proposed by Ibarra et al. (2005) was assigned to both. Structural damping of $\zeta = 2\%$ was assumed for the steel and $\zeta = 5\%$ for the RC frame, modelled according to the recommendations of Zareian and Medina (2010). Geometric non-linearity in the form of $P - \Delta$ effects was also taken into account. The SPO curves of both frames, obtained using first-mode-

proportional load patterns, are shown in Figure 12, along with the equivalent SDoF backbone of their SPO2FRAG elaboration.

For the purpose of running IDA with these numerical structural models, a set of eighty recorded accelerograms was assembled. This set includes the twenty-two ground motions of the far-field set in FEMA-P695 (FEMA, 2009), which was enriched by another eighteen records from the Engineering Strong Motion database (http://esm.mi.ingv.it). Both recorded horizontal components at each station are applied to the plane structural models separately. Overall, the ground motion suite includes records from events with magnitude from 6.0 to 7.6, recorded at distances from 5 to 50 km on firm soil (EC 8 classification A, B or C), not containing relevant directivity effects and exhibiting PGA in the range from 0.12 to 0.90g.
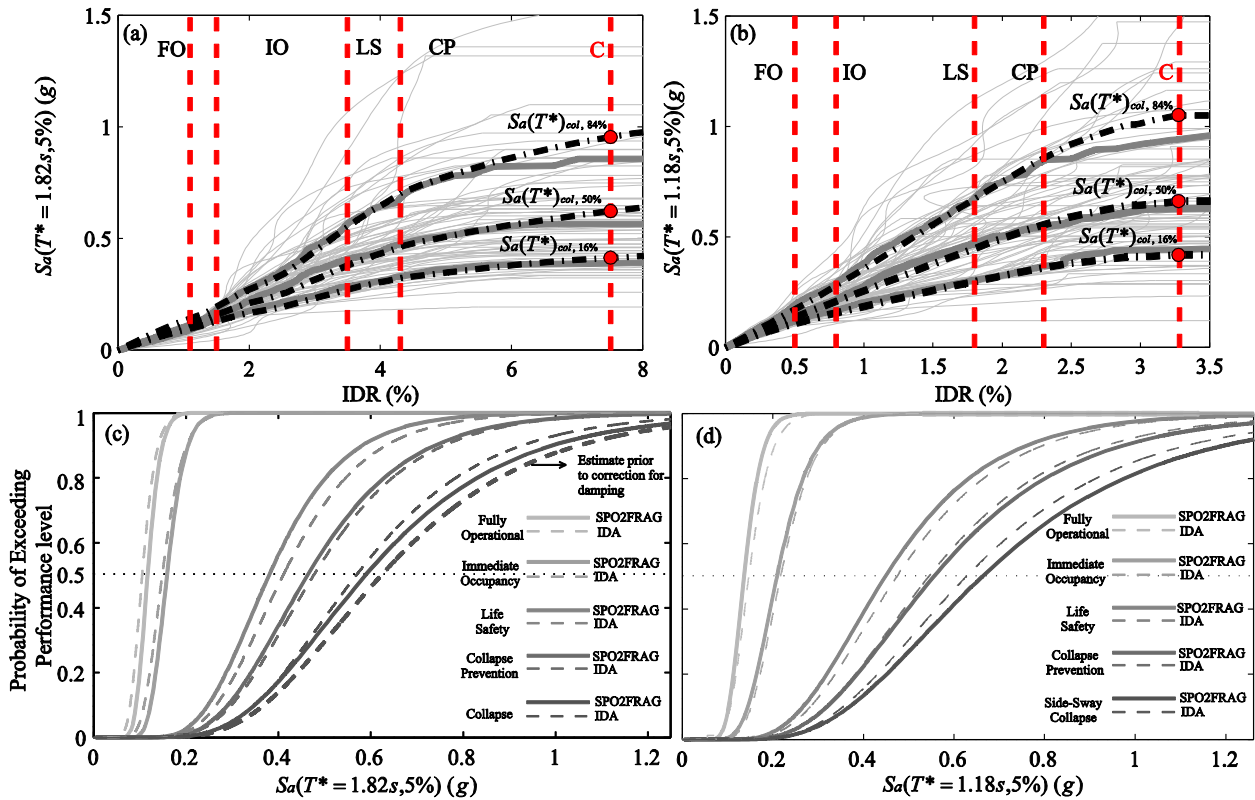

Figure 13. Analytical IDA curves and corresponding SPO2FRAG predictions for (a) the four-storey steel MRF and (b) the six-storey RC-MRF. Comparison of IDA- and SPO2FRAG-based lognormal fragility functions per limit state for (c) the four-storey steel MRF and (d) the six-storey RC-MRF.

4.2 Comparison of IDA- and SPO2FRAG-based fragility estimates

Both structures were subjected to IDA using the set of eighty accelerograms described above, while their SPO curves were used to simultaneously run fragility estimates in SPO2FRAG. In order to limit the number of required analyses to reasonable levels, IDA was run using the hunt-and-fill algorithm proposed by Vamvatsikos and Cornell (2004). For both structures, limit state exceedance thresholds were defined in terms of IDR. Immediate occupancy, life safety and collapse prevention IDR thresholds were determined using the SPO results, by imposing the maximum plastic rotation acceptance criteria of FEMA-356 to the critical elements (first-storey columns). The fully operational threshold was set to 0.5% IDR for the RC-MRF and near the nominal yield for the steel MRF. Global collapse was left to be automatically determined by SPO2FRAG based on the predicted flat-line heights of the IDA fractiles for the RC-MRF (thus mainly corresponding to side-sway collapse) while for the steel MRF it was set to the IDR corresponding to 50% loss of strength measured on the SPO curve, by using the relevant in-built tool (e.g., Figure 8) to capture additional modes of failure that

may be expected to appear at such large drifts. Furthermore, for the steel four-storey MRF, Γ_{eff} according to Eq.(6) was employed due to the more flexible frame's higher-mode sensitivity and the correction due to $\zeta \neq 5\%$ was applied according to Eq. (10). Finally, the default choice of Eq. (8) was employed for the estimation of dispersion in both cases (see also Figure 10).

In Figure 13 the IDA results, for both structures, can be seen with the SPO2FRAG predictions superimposed. Additionally, the fragility curves obtained for each limit state by SPO2FRAG are presented for comparison with the same curves derived from the IDA results using Eq. (14) for the estimate of β, where the index $i = \{1, ..., N\}$ refers to the response to the i-th accelerogram.

$$\beta = \sqrt{\frac{1}{N-1} \cdot \sum_{i=1}^{N} \left[\left(\ln\left(Sa_{C,i}^{LS}\right) - \ln\left(Sa_{C,50\%}^{LS}\right) \right)^2 \right]} \tag{14}$$

The corresponding parameter estimates are provided in Tables 1 and 2. In order to get an appreciation of the effect that the choice of employing Γ_{eff} (a choice made for the case of the steel MRF alone) bears on these results, it is mentioned that the SPO2FRAG prediction of median intensity at collapse for the four-storey steel MRF using Γ is 0.60g (compare with 0.59g in Table 1 resulting from using Γ_{eff} instead). On the other hand, for the six-storey RC-MRF, the choice of using Γ_{eff} or Γ leaves the median collapse intensity practically unaffected.

Table 1. Lognormal fragility function parameter estimates from SPO2FRAG and IDA and corresponding annual limit-state exceedance rates (events/year) for the four-storey steel MRF assumed to be situated at L'Aquila.

Limit state	$\exp(\eta)$ (IDA)	β (IDA)	$\exp(\eta)$ (SPO2FRAG)	β (SPO2FRAG)	λ_f (IDA)	λ_f (SPO2FRAG)
Fully Operational	0.105 g	0.223	0.117 g	0.189	$6.7 \cdot 10^{-3}$	$5.7 \cdot 10^{-3}$
Immediate Occupancy	0.149 g	0.239	0.159 g	0.197	$4.0 \cdot 10^{-3}$	$3.6 \cdot 10^{-3}$
Life Safety	0.410 g	0.340	0.379 g	0.334	$7.1 \cdot 10^{-4}$	$8.3 \cdot 10^{-4}$
Collapse Prevention	0.476 g	0.364	0.463 g	0.364	$5.3 \cdot 10^{-4}$	$5.7 \cdot 10^{-4}$
Collapse	0.569 g	0.383	0.589 g	0.409	$3.7 \cdot 10^{-4}$	$3.6 \cdot 10^{-4}$

Table 2. Lognormal fragility function parameter estimates from SPO2FRAG and IDA and corresponding annual limit-state exceedance rates (events/year) for the six-storey RC-MRF assumed to be situated at Ancona.

Limit state	$\exp(\eta)$ (IDA)	β (IDA)	$\exp(\eta)$ (SPO2FRAG)	β (SPO2FRAG)	λ_f (IDA)	λ_f (SPO2FRAG)
Fully Operational	0.147 g	0.256	0.136 g	0.226	$1.3 \cdot 10^{-3}$	$1.5 \cdot 10^{-3}$
Immediate Occupancy	0.217 g	0.278	0.208 g	0.288	$5.5 \cdot 10^{-4}$	$6.1 \cdot 10^{-4}$
Life Safety	0.473 g	0.403	0.448 g	0.407	$9.4 \cdot 10^{-5}$	$1.1 \cdot 10^{-4}$
Collapse Prevention	0.544 g	0.421	0.555 g	0.434	$6.7 \cdot 10^{-5}$	$6.6 \cdot 10^{-5}$
Collapse	0.627 g	0.446	0.662 g	0.458	$4.9 \cdot 10^{-5}$	$4.4 \cdot 10^{-5}$

4.3 Comparing SPO2FRAG and IDA results in the context of seismic risk assessment.

In order to better appreciate the agreement between the SPO2FRAG and IDA results, integration with seismic hazard was performed by plugging Eq.(3) into Eq. (1), thus obtaining estimates of the annual exceedance rate for each limit state (without considering estimation uncertainty for the sake of simplicity).
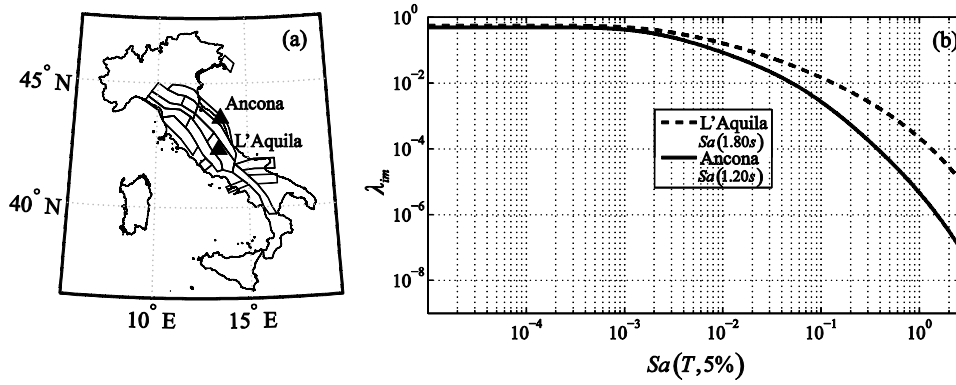
Figure 14. Map of Italy showing the two sites of interest and the seismic sources considered for the seismic hazard calculations (a) and calculated hazard curves to be integrated with structural fragility of the case-study examples (b): annual exceedance rate of $Sa(1.80s, 5\%)$ at L'Aquila and the same for $Sa(1.20s, 5\%)$ at Ancona. As the Akkar and Bommer (2010) ground motion prediction equation is employed, the closest available periods to T^* are used for each case to avoid interpolation.

To be able to do so, it was assumed that the 4-storey steel MRF is situated at a site near the Italian city of L'Aquila and the 6-storey RC-MRF at a site near the Italian port-town of Ancona. For both of these sites, the seismic hazard was calculated with the aid of the REASSESS software (Iervolino et al., 2016b), assuming firm soil conditions. The hazard at these sites was calculated using the seismic source model from Meletti et al. (2008), seismicity rates from Barani et al. (2009,2010) and the ground motion prediction equation proposed by Akkar and Bommer (2010). The annual exceedance rates of the 5%-damped spectral acceleration at T^* are shown in Figure 14. The calculated annual rates of limit-state exceedance are included among the results reported in Tables 1 and 2. The good agreement between the SPO2FRAG and analytically-derived estimate is evident.

5. CONCLUSIONS

The present article introduced SPO2FRAG, an interactive MATLAB®-coded PBEE tool useful for approximate, computer-aided calculation of building fragility functions based on static pushover analysis. SPO2FRAG (available online at http://wpage.unina.it/iuniervo under a Creative Commons license: attribution – non commercial – non derived) comes as a standalone application, with various intercommunicating modules nested behind a user-friendly graphical user interface.

The software uses SPO results as a vehicle to obtain an equivalent SDoF representation of the non-linear structure and subsequently goes on to employ the SPO2IDA algorithm to avoid the need for time-consuming dynamic analysis for obtaining probabilistic estimates of seismic response. A series of specifically-developed tools are then called upon to effect and SDoF-to-MDoF response transformation, culminating in the calculation of fragility parameters and going as far as providing information related to the underlying estimation uncertainty. In the preceding sections, the workflow of a complete SPO2FRAG operation was outlined from both the user-end and the software-end. A practical user guide can be found online at http://wpage.unina.it/iuniervo/ . Summarizing, the software is characterized by versatility, accepting as input static pushover results obtained from the structural analysis software package of the user's choice and allowing the user to control the IDA simulation and fragility estimation procedure at its various steps and intervene where one deems necessary.

The viability of SPO2FRAG as a calculation tool was demonstrated by means of two case-study examples, where fragility functions estimated using the software were compared and found in agreement with the analytical solution involving IDA. It was therefore shown that, for regular,

symmetric frames (i.e., cases of fist-mode dominated structures for which the fundamental assumptions behind static pushover analysis apply) SPO2FRAG is able to provide expedient solutions to the issue of analytical, building-specific seismic fragility estimation, under the assumptions behind IDA.

ACKNOWLEDGEMENTS

REFERENCES

Adam C, Ibarra LF (2015) Seismic collapse assessment. In: Earthquake Engineering Encyclopedia (Beer M, Kougioumtzoglou IA, Patelli E, Siu-Kui Au I, eds), Vol. 3, pp. 2729-2752, Berlin Heidelberg: Springer.

Akkar S, Bommer JJ (2010) Empirical equations for the prediction of PGA, PGV and spectral accelerations in Europe, the Mediterranean region and the Middle East. Seismological Research Letters, 81(2), 195-206.

ASCE (2000) FEMA-356: Prestandard and commentary for the seismic rehabilitation of buildings. Developed by ASCE for FEMA, Washington, D.C.

ASCE (2007) ASCE/SEI 41-06: Seismic rehabilitation of existing buildings. Reston, VA.

Baker JW (2015) Efficient analytical fragility function fitting using dynamic structural analysis. Earthquake Spectra, 31(1), 579-599.

Baltzopoulos G, Chioccarelli E, Iervolino I (2015) The displacement coefficient method in near-source conditions. Earthquake Engineering and Structural Dynamics, 44(7), 1015-1033.

Barani S, Spallarossa D, Bazzurro P (2009) Disaggregation of probabilistic ground-motion hazard in Italy. Bulletin of the Seismological Society of America, 99, 2638-2661.

Barani S, Spallarossa D, Bazzurro P (2010) Erratum to disaggregation of probabilistic ground-motion hazard in Italy. Bulletin of the Seismological Society of America, 100, 3335-3336.

Bazzuro P, Cornell CA, Shome N, Carballo JE (1998) Three proposals for characterizing MDOF non-linear seismic response. Journal of Structural Engineering, 124, 1281-1289.

BSSC (1997) FEMA-273: NEHRP guidelines for the seismic rehabilitation of buildings. Developed by ATC for FEMA, Washington, D.C.

Calvi GM, Pinho R, Magenes G, Bommer JJ, Restrepo-Vélez LF, Crowley H (2006) Development of seismic vulnerability assessment methodologies over the past 30 years. ISET Journal of Earthquake Technology: 43(3), 75-104.

CEN (2004) EN 1998-1 Design of structures for earthquake resistance – Part 1: General rules seismic actions and rules for buildings, European Committee for Standardization, Brussels.

Cornell CA, Jalayer F, Hamburger RO, Foutch DA (2002) The probabilistic basis for the SAC/FEMA steel moment frame guidelines. Journal of Structural Engineering, 128, 526-533.

Cornell CA, Krawinkler H (2000) Progress and challenges in seismic performance assessment. PEER Center News 3(2), 1-3.

De Luca F, Vamvatsikos D, Iervolino I (2013) Near-optimal piecewise linear fits of static pushover capacity curves for equivalent SDOF analysis. Earthquake Engineering and Structural Dynamics: 42(4), 523-543.

Dolsek M (2009) Incremental dynamic analysis with consideration of modelling uncertainties. Earthquake Engineering and Structural Dynamics, 38(6), 805-825.

Efron B (1982) The jackknife, the bootstrap and other resampling plans. In CBMS-NSF, Regional conference series in applied mathematics, Society for industrial and applied mathematics, Philadelphia, US.

Fajfar P (2000) A nonlinear analysis method for performance based seismic design. Earthquake Spectra, 16(3), 573-592.

FEMA (2005) FEMA-440: Improvement of nonlinear static seismic analysis procedures. Prepared by ATC for FEMA, Washington D.C.

FEMA (2009) FEMA-P695: Quantification of Building Seismic Performance Factors. Federal Emergency Management Agency, Washington D.C.

FEMA (2012) FEMA-58-1: Seismic performance assessment of buildings volume 1 – Methodology. Prepared by ATC for FEMA, Washington D.C.

Fragiadakis M, Vamvatsikos D (2010) Fast performance uncertainty estimation via pushover and approximate IDA. Earthquake Engineering and Structural Dynamics, 39(6), 683-703.

Fragiadakis M, Vamvatsikos D, Ascheim M (2014) Application of nonlinear static procedures for seismic assessment of regular RC moment frame buildings. Earthquake Spectra, 30(2), 767–794.

Han SW, Moon K, Chopra AK (2010) Application of MPA to estimate the probability of collapse of structures. Earthquake Engineering and Structural Dynamics: 39, 1259-1278.

Haselton CB, Deierlein GG (2007) Assessing seismic collapse safety of modern reinforced concrete moment-frame buildings. PEER Report 2007/08, Pacific Earthquake Engineering Center, University of California, Berkley.

Haselton CB, Liel AB, Deierlein GG, Dean BS, Chou JS (2011) Seismic collapse safety of reinforced concrete buildings. I: Assessment of ductile moment frames. Journal of Structural Engineering, 137(4), 481-491.

Ibarra LF, Medina RA, Krawinkler H (2005) Hysteretic models that incorporate strength and stiffness deterioration. Earthquake Engineering and Structural Dynamics, 34, 1489-1511.

Iervolino I, Baltzopoulos G, Vamvatsikos D, Baraschino R (2016a) SPO2FRAG v1.0: software for PUSHOVER-BASED derivation of seismic fragility curves. Proceedings of the VII European Congress on Computational Methods in Applied Sciences and Engineering, ECCOMAS, Crete Island, Greece, 5–10 June.

Iervolino I, Chioccarelli E, Cito P (2016b) REASSESS V1.0: a computationally-efficient software for probabilistic seismic hazard analysis. Proc. of VII European Congress on Computational Methods in Applied Sciences and Engineering, ECCOMAS, Crete Island, Greece, 5–10 June.

Iervolino I, Cornell CA (2005) Record selection for nonlinear seismic analysis of structures. Earthquake Spectra, 21(3), 685-713.

Jalayer F, Cornell CA (2003) A technical framework for probability-based demand and capacity factor design (DCFD) seismic formats. PEER Report 2003/08, Pacific Earthquake Engineering Center, University of California, Berkley.

Kohrangi M., Vamvatsikos D., Bazzurro P. (2017). Site dependence and record selection schemes for building fragility and regional loss assessment. *Earthquake Engineering and Structural Dynamics.* DOI: 10.1002/eqe.2873

Krawinkler H, Seneviratna GDPK (1998) Pros and Cons of a Pushover Analysis of Seismic Performance Evaluation. Engineering Structures, 20(4-6), 452-464.

Kwong NS, McGuire RK, Chopra AK (2015) A framework for the evaluation of ground motion selection and modification procedures. Earthquake Engineering and Structural Dynamics, 44(5), 795-815.

Lignos DG, Krawinkler H (2011) Deterioration modelling of steel components in support of collapse prediction of steel moment frames under earthquake loading. Journal of Structural Engineering, 137(11), 1291-1302.

Luco N, Cornell CA (2007) Structure-specific scalar intensity measures for near-source and ordinary earthquake ground motions. Earthquake Spectra: 23(2), 357-392.

McKenna F, Fenves GL, Scott MH, Jeremic B (2000) Open System for Earthquake Engineering Simulation (OpenSees). Pacific Earthquake Engineering Research Center, University of California, Berkeley, CA.

Meleti C, Galadini F, Valensise C, Stucchi M, Basili R, Barba S, Vannucci G, Boschi E (2008) A seismic source zone model for the seismic hazard assessment of the Italian territory. Tectonophysics, 450, 85-108.

Moehle JP (1992) Displacement-based design of RC structures subject to earthquakes, Earthquake Spectra, 8(3): 403–428.

Mood AM, Graybill FA, Boes DC (1974) Introduction to the theory of statistics. Mc-Graw Hill, New York.

NIST (2010) Evaluation of the FEMA P-695 methodology for quantification of building performance factors. Report No. NIST GCR 10-917-8. Prepared for the US National Institute of Standards and Technology by the NEHRP Consultants Joint Venture, Gaithersburg, MD.

SEAOC (1995) VISION 2000: Performance based seismic engineering of buildings, San Francisco.

Shome N, Cornell CA (1999) Probabilistic seismic demand analysis of nonlinear structures. Doctoral Dissertation, Stanford University, CA.

Vamvatsikos D (2014) Seismic performance uncertainty estimation via IDA with progressive accelerogram-wise latin hypercube sampling. Journal of Structural Engineering, 140(8), A4014015.

Vamvatsikos D, Cornell CA (2002) Incremental dynamic analysis. Earthquake Engineering and Structural Dynamics: 31, 491-514.

Vamvatsikos D, Cornell CA (2004) Applied incremental dynamic analysis. Earthquake Spectra: 20(2), 523–553.

Vamvatsikos D, Cornell CA (2005) Direct estimation of seismic demand and capacity of multiple-degree-of-freedom systems through incremental dynamic analysis of single degree of freedom approximation. Journal of Structural Engineering: 131, 589-599.

Vamvatsikos D, Cornell CA (2006) Direct estimation of the seismic demand and capacity of oscillators with multi-linear static pushovers through IDA. Earthquake Engineering and Structural Dynamics: 35, 1097–1117.

Vamvatsikos D, Fragiadakis M (2010) Incremental dynamic analysis for estimating seismic performance uncertainty and sensitivity. Earthquake Engineering and Structural Dynamics, 39(2): 141-163.

Katsanos EI, Vamvatsikos D (2017) Yield Frequency Spectra and seismic design of code-compatible RC structures: an illustrative example. Earthquake Engineering and Structural Dynamics (in press).

Vidic T, Fajfar P, Fischinger M (1994) Consistent inelastic design spectra: strength and displacement. Earthquake Engineering and Structural Dynamics, 23, 507-521.

Zareian F, Medina R (2010) A practical method for proper modeling of structural damping in inelastic plane structural systems. Computers and Structures, 88(1-2), 45-53.